

Testing the 2-TeV Resonance with Trileptons

Arindam Das^a, Natsumi Nagata^b, Nobuchika Okada^a

^a*Department of Physics and Astronomy, University of Alabama,
Tuscaloosa, Alabama 35487, USA*

^b*William I. Fine Theoretical Physics Institute, School of Physics and Astronomy,
University of Minnesota, Minneapolis, Minnesota 55455, USA*

Abstract

The CMS collaboration has reported a 2.8σ excess in the search of the $SU(2)_R$ gauge bosons decaying through right-handed neutrinos into the two electron plus two jets ($eejj$) final states. This can be explained if the $SU(2)_R$ charged gauge bosons W_R^\pm have a mass of around 2 TeV and a right-handed neutrino with a mass of $\mathcal{O}(1)$ TeV mainly decays to electron. Indeed, recent results in several other experiments, especially that from the ATLAS diboson resonance search, also indicate signatures of such a 2 TeV gauge boson. However, a lack of the same-sign electron events in the CMS $eejj$ search challenges the interpretation of the right-handed neutrino as a Majorana fermion. Taking this situation into account, in this paper, we consider a possibility of explaining the CMS $eejj$ excess based on the $SU(2)_L \otimes SU(2)_R \otimes U(1)_{B-L}$ gauge theory with pseudo-Dirac neutrinos. We find that both the CMS excess events and the ATLAS diboson anomaly can actually be explained in this framework without conflicting with the current experimental bounds. This setup in general allows sizable left-right mixing in both the charged gauge boson and neutrino sectors, which enables us to probe this model through the trilepton plus missing-energy search at the LHC. It turns out that the number of events in this channel predicted in our model is in good agreement with that observed by the CMS collaboration. We also discuss prospects for testing this model at the LHC Run-II experiments.

1 Introduction

The CMS collaboration announced that they observed excess events in their search for new massive charged gauge bosons (W_R^\pm) associated with the the $SU(2)_R$ gauge symmetry which decay into two leptons and dijet through heavy right-handed neutrinos [1]. The excess was found in the invariant mass distribution of the two electrons and dijet ($eejj$) final states around 2 TeV, whose significance is 2.8σ . This signal, if confirmed, certainly implies the presence of TeV-scale new physics. Various models have been proposed so far to interpret this CMS excess; see, *e.g.*, Refs. [2–9]. Among them, models based on the $SU(2)_L \otimes SU(2)_R \otimes U(1)_{B-L}$ gauge theory [10] are the simplest and most promising candidates, since they contain right-handed neutrinos and W_R^\pm as their indispensable ingredients. Indeed, such models have attracted a lot of attentions recently [5–9, 11] since they can explain possible anomalies observed in other (totally independent) experiments, such as a 3.4σ excess in the ATLAS diboson resonance search [12], an around 2σ excess in the CMS dijet resonance search [13], and a 2.2σ excess in the $W^\pm h$ channel where W^\pm decays leptonically and the Higgs boson h decays into $b\bar{b}$ [14]. All of these results indicate the presence of W_R^\pm with a mass of around 2 TeV.

If such a TeV-scale W_R^\pm exists, in the $SU(2)_L \otimes SU(2)_R \otimes U(1)_{B-L}$ models, we also expect that there are right-handed neutrinos whose masses are of $\mathcal{O}(1)$ TeV. The presence of these right-handed neutrinos is desirable since we can exploit them to explain the CMS $eejj$ excess events. An important caveat here is, however, that the CMS collaboration observed only one same-sign electron event among all 14 $eejj$ events [1]. This observation disfavors the conventional $SU(2)_L \otimes SU(2)_R \otimes U(1)_{B-L}$ model with an $SU(2)_R$ triplet Higgs field; in this case, right-handed neutrinos are Majorana fermions, with which we expect the same number of same-sign dilepton events as that of the opposite-sign ones. In addition, TeV-scale right-handed Majorana neutrinos are stringently restricted by the recent ATLAS [15] and CMS searches [16, 17] in the same-sign leptons plus dijet final states. Therefore, it is required to extend this conventional model so that it evades the above problems.

The inverse seesaw [18] mechanism offers a promising way to reconcile the difficulties. In this mechanism, three singlet fermions are added to the neutrino sector on top of right-handed neutrinos. Then, small lepton-number violation in the singlet mass terms results in three light left-handed neutrinos as well as heavy pseudo-Dirac neutrinos. Since a neutrino which couples to W_R^\pm is a pseudo-Dirac fermion, the lepton number is approximately conserved in the process of W_R^\pm decaying to the neutrino, which accounts for a lack of same-sign electron events in the CMS $eejj$ signals. Moreover, this mechanism has an advantage in explaining small neutrino masses with TeV-scale $SU(2)_L \otimes SU(2)_R \otimes U(1)_{B-L}$ symmetry. With such a low-scale symmetry-breaking of $SU(2)_R$, the ordinary type-I seesaw mechanism [19] can yield small neutrino masses only with very small Yukawa couplings unless a specific mass structure is assumed [20], while the inverse seesaw mechanism allows the couplings to be sizable. This feature is favorable when the model is considered in the framework of grand unification [21] like $SO(10)$ models [22].

In this paper, we consider an $SU(2)_L \otimes SU(2)_R \otimes U(1)_{B-L}$ model that is extended to

accommodate the inverse seesaw mechanism. For recent work which considers a similar model, see Ref. [6]. It is found that our model can actually realize the right number of $eejj$ signals observed in the CMS experiment [1]. A characteristic feature of our model is that it allows sizable left-right mixing in both the charged gauge boson and neutrino sectors. Indeed, such a significant W - W_R mixing is favored from the viewpoint of the ATLAS diboson excess [12]. Moreover, the inverse seesaw mechanism allows a large left-right neutrino mixing while keeping neutrino masses tiny. In the presence of the left-right mixing, a heavy Dirac neutrino can decay into not only the two leptons plus two jets final states via a virtual W_R exchange, but also into a lepton plus a gauge/Higgs boson channels via the left-right mixing. Such decay processes yield a trilepton plus missing energy signature, which is regarded as the golden channel for probing heavy Dirac neutrinos at the LHC [23–27]. We study the prediction of our model in this channel, and find that the predicted number of events is in good agreement with the result given by the CMS collaboration [28]. We further discuss the future prospects for testing this model at the next stage of the LHC run.

This paper is organized as follows. In the next section, we first describe our model which we consider in this work. In Sec. 3, we show the decay branching ratios of W_R and heavy Dirac neutrinos. Then, we study the collider signatures of our model in Sec. 4. Section 5 is devoted to conclusion and discussions.

2 Model

To begin with, we propose a model based on the $SU(3)_C \otimes SU(2)_L \otimes SU(2)_R \otimes U(1)_{B-L}$ gauge symmetry which has the structure of the inverse seesaw mechanism [18] in the neutrino sector. As in the Standard Model (SM), left-handed quarks and leptons form $SU(2)_L$ doublet fields:

$$Q_{L_i} = \begin{pmatrix} u_{L_i} \\ d_{L_i} \end{pmatrix}, \quad L_{L_i} = \begin{pmatrix} \nu_{L_i} \\ e_{L_i} \end{pmatrix}, \quad (1)$$

where $i = 1, 2, 3$ denotes the generation index. On the other hand, right-handed fermions are embedded into the $SU(2)_R$ fundamental representation as

$$Q_{R_i} = \begin{pmatrix} u_{R_i} \\ d_{R_i} \end{pmatrix}, \quad L_{R_i} = \begin{pmatrix} N_{R_i} \\ e_{R_i} \end{pmatrix}. \quad (2)$$

In addition, we introduce three gauge-singlet fermions S_{L_i} , which lead to chiral partner fields of N_{R_i} as we see below.

The Higgs sector of this model contains two Higgs multiplets. One is an $SU(2)_L \otimes SU(2)_R$ bi-doublet scalar field with zero $B - L$ charge, which breaks the electroweak symmetry and thus plays a role of the SM Higgs field. We denote it by Φ and its vacuum expectation value (VEV) by

$$\langle \Phi \rangle = \begin{pmatrix} v_u & 0 \\ 0 & v_d \end{pmatrix}, \quad (3)$$

with $v = \sqrt{v_u^2 + v_d^2} \simeq 174$ GeV. Moreover, to break the $SU(2)_R$ symmetry, we introduce an $SU(2)_R$ doublet Higgs field H_R with a $B - L$ charge $+1$, whose VEV is given by

$$\langle H_R \rangle = \begin{pmatrix} 0 \\ v_R \end{pmatrix}. \quad (4)$$

This breaks $SU(2)_L \otimes SU(2)_R \otimes U(1)_{B-L}$ to $SU(2)_L \otimes U(1)_Y$.

With these particle contents, the interaction terms are generically given as follows:

$$\begin{aligned} \mathcal{L}_{\text{int}} = & -y_{ij}^Q \bar{Q}_{R_i} \Phi Q_{L_j} - \tilde{y}_{ij}^Q \bar{Q}_{R_i} \tilde{\Phi} Q_{L_j} - y_{ij}^L \bar{L}_{R_i} \Phi L_{L_j} - \tilde{y}_{ij}^L \bar{L}_{R_i} \tilde{\Phi} L_{L_j} \\ & - f_{ij} \bar{L}_{R_i} i\sigma_2 H_R^* S_{L_j} - \frac{1}{2} \mu_{ij} \bar{S}_{L_i}^c S_{L_j} + \text{h.c.}, \end{aligned} \quad (5)$$

where $\tilde{\Phi} \equiv \sigma_2 \Phi^* \sigma_2$ with σ_a ($a = 1, 2, 3$) being the Pauli matrices, and c indicates the charge conjugation. Note that the Majorana mass terms for right-handed neutrinos N_{R_i} are forbidden by the $SU(2)_R$ gauge symmetry. After the above Higgs fields develop the VEVs, these interaction terms lead to the mass terms of the fermions. Here we assume that these Yukawa couplings and the VEVs are appropriately chosen so that the resultant mass terms agree to the observed quark and lepton masses as well as the Cabibbo–Kobayashi–Maskawa (CKM) matrix elements.¹ The mass matrix of the neutrino sector is written as

$$\mathcal{L}_{\text{mass}} = -\frac{1}{2} \bar{\psi}_i^c \mathcal{M}_{ij} \psi_j + \text{h.c.}, \quad (6)$$

where $\psi_i \equiv (\nu_{L_i}, N_{R_i}^c, S_{L_i})$, and

$$\mathcal{M}_{ij} = \begin{pmatrix} 0 & M_D & 0 \\ M_D^T & 0 & M_N^T \\ 0 & M_N & \mu \end{pmatrix}_{ij} \equiv \begin{pmatrix} 0 & \mathcal{M}_D \\ \mathcal{M}_D^T & \mathcal{M}_N \end{pmatrix}_{ij}, \quad (7)$$

with

$$\begin{aligned} (M_D^T)_{ij} &= y_{ij}^L v_u + \tilde{y}_{ij}^L v_d, \\ (M_N^T)_{ij} &= f_{ij} v_R. \end{aligned} \quad (8)$$

Notice that the Majorana mass terms for N_{R_i} are still not produced due to the choice of the Higgs field that breaks the $SU(2)_R$ symmetry.² Here, we assume a hierarchical

¹Note that the structure of the quark/lepton Yukawa couplings is the same as that of the generic two-Higgs doublet model. Thus, we have more degrees of freedom for the Yukawa couplings than those in, *e.g.*, the type-II two-Higgs doublet model. These extra degrees of freedom are actually desirable since we can choose the Yukawa couplings to account for the observed fermion masses and mixing even though we take $v_u/v_d = \mathcal{O}(1)$; if we instead consider the type-II two-Higgs doublet model like structure, then v_u/v_d should be equal to m_t/m_b in order to explain the observed top-bottom mass ratio.

²If we used an $SU(2)_R$ triplet Higgs field with two unit of the $B - L$ charge to break the $SU(2)_R$ symmetry, then we would generically obtain Majorana mass terms for N_{R_i} .

structure among the mass parameters in the matrix, *i.e.*, $|\mu_{ij}| \ll |(M_D)_{ij}| \ll |(M_N)_{ij}|$. The mass matrix \mathcal{M} can be block diagonalized by means of a unitary matrix. We obtain the mass matrix for light neutrinos as

$$M_\nu \simeq -\mathcal{M}_D \mathcal{M}_N^{-1} \mathcal{M}_D^T \simeq M_D M_N^{-1} \mu (M_N^T)^{-1} M_D^T, \quad (9)$$

while the other two classes of mass eigenvalues are given by $M_N \mp \mu/2$. The latter can be regarded as pseudo-Dirac neutrinos for $|\mu| \ll M_N$. Notice that small neutrino masses are guaranteed by the smallness of $|\mu|$, and these masses vanish in the limit of $\mu \rightarrow 0$. In this limit, the theory recovers the lepton-number symmetry, which results in three massless neutrinos and three heavy Dirac neutrinos. Since the μ_{ij} term in Eq. (5) does not break any symmetry in our model, μ_{ij} in principle can have arbitrary large value. We do not specify any mechanism to obtain a small μ in this paper, though there have been several proposals to explain the smallness of μ by exploiting spontaneous breaking of the lepton-number symmetry [29], extra dimensions [30], or generation of μ through radiative corrections [31]. Finally, we note in passing that an extremely small $|\mu|$ allows the lepton Yukawa couplings f_{ij} to be sizable, which then indicates that the left-right mixing in the neutrino sector can also be significant.

The VEV of H_R gives masses to not only heavy neutrinos but also gauge bosons associated with the broken symmetries. After the symmetry breaking, we have massive charged and neutral gauge bosons, W_R^\pm and Z_R , whose masses are given by

$$m_{W_R} \simeq \frac{g_R}{\sqrt{2}} v_R, \quad m_{Z_R} \simeq \frac{\sqrt{g_R^2 + g_{B-L}^2}}{\sqrt{2}} v_R, \quad (10)$$

respectively. Here, the $SU(2)_R$ gauge coupling constant g_R and the $B-L$ gauge coupling constant g_{B-L} are related to the $U(1)_Y$ gauge coupling constant g' by

$$\frac{1}{g'^2} = \frac{1}{g_R^2} + \frac{1}{g_{B-L}^2}, \quad (11)$$

which follows from

$$Y = T_R^3 + \frac{B-L}{2}, \quad (12)$$

with Y , T_R^A , and $B-L$ denote the hypercharge, the $SU(2)_R$ generators, and the $B-L$ charge, respectively. From the relation (11), we find that there is a lower bound on the value of g_R to keep the $B-L$ coupling perturbative; for instance, $g_{B-L} < 1$ (4π) leads to $g_R \gtrsim 0.39$ (0.36).

As mentioned in Sec. 1, recently there have been various experimental observations which indicate the presence of W_R^\pm with a mass of around 2 TeV. Motivated by these observations, throughout this paper, we assume $m_{W_R} \sim 2$ TeV. In this case, we can predict the mass of Z_R as a function of g_R according to Eqs. (10) and (11). In Fig. 1, we plot m_{Z_R} as a function of g_R . Here, we set $m_{W_R} = 2$ TeV. Currently, the most stringent limit on Z_R is given by the ATLAS collaboration using the 3.2 fb^{-1} data set at the center-of-mass energy of $\sqrt{s} = 13$ TeV [32] (see also the CMS result [33]). According to the

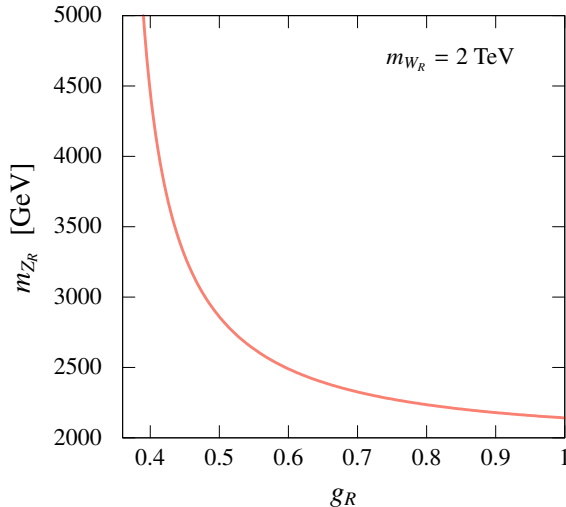


Figure 1: Mass of Z_R , m_{Z_R} , as a function of the $SU(2)_R$ gauge coupling g_R . Here, we set $m_{W_R} = 2$ TeV.

ATLAS result, the production cross section of Z_R times its branching fraction into two leptons ℓ^\pm ($\ell = e, \mu$), $\sigma(Z_R)\text{BR}(\ell^+\ell^-)$ should be less than about 1 fb, which gives a lower limit on the Z_R mass of a several TeV. This limit can easily be avoided if one takes $g_R \simeq 0.4$.

Since $m_{W_R} \sim 2$ TeV means $v_R = \mathcal{O}(1)$ TeV, Eq. (8) tells us that heavy pseudo-Dirac neutrinos also have masses of $\mathcal{O}(1)$ TeV. To explain the CMS excess, we take one of these heavy neutrinos to have a mass lighter than m_{W_R} and the others to have masses heavier than m_{W_R} so that they do not participate in the decay of W_R . We denote the former by N_1 and the latter by N_2 and N_3 in what follows. In addition, we assume that N_1 mainly couples to electron; *i.e.*, its couplings with μ and τ leptons are negligible. In this setup, W_R decays into a pair of right-handed quarks, WZ , Wh , or a N_1 plus an electron. In the last case, the produced N_1 subsequently decays into an electron plus quarks via the exchange of a virtual W_R^\pm . It can also decay into three leptons or a lepton plus two quarks via the W^\pm , Z , or the Higgs boson exchange if N_1 has a sizable left-handed neutrino component or W - W_R mixing is rather large. Relevant formulae for the decay processes are summarized in the subsequent section.

Finally, we give a brief discussion about the constraint on W_R coming from flavor physics. In this model, flavor-changing-neutral-current (FCNC) processes can be induced by the exchange of W_R ,³ which are severely restricted from the low-energy precision flavor measurements. Among them, the measurement of the K_L - K_S mass difference gives the

³ As we discussed above, the structure of the Yukawa sector in our model is similar to that in the generic two-Higgs-doublet model. Thus, FCNC processes may also be induced by the exchange of the additional Higgs bosons in general. In this paper, we simply assume that the Yukawa couplings in our model are appropriately aligned so that FCNC processes generated by the Higgs exchange are sufficiently suppressed.

most stringent bound on m_{W_R} , which is roughly given by [34]

$$m_{W_R} \gtrsim \left(\frac{g_R}{g_L}\right) \times 2.5 \text{ TeV} \simeq \left(\frac{g_R}{0.4}\right) \times 1.5 \text{ TeV} . \quad (13)$$

Hence, W_R with a mass of around 2 TeV is still allowed by this bound when we take $g_R \simeq 0.4$.

3 Decay Branching Fractions

Here, we first summarize formulae relevant to the calculation of the partial decay widths of W_R^\pm and N_1 . As mentioned above, W_R decays into a pair of right-handed quarks, WZ , Wh , or a N_1 plus an electron. Among them, the WZ and Wh decay processes occur via the mixing of W_R with W boson. Therefore, we begin with the discussion on the W - W_R mixing in our model. W_R mixes with W boson after the bi-doublet Higgs field Φ acquires a VEV. The mass matrix of these gauge bosons is given by

$$\mathcal{L}_{\text{mass}} = (W_L^- \ W_R^-) \begin{pmatrix} \frac{g_L^2 v^2}{2} & -\frac{g_L g_R v^2 \sin 2\beta}{2} \\ -\frac{g_L g_R v^2 \sin 2\beta}{2} & \frac{g_R^2}{2} \{v_R^2 + v^2\} \end{pmatrix} \begin{pmatrix} W_L^+ \\ W_R^+ \end{pmatrix}, \quad (14)$$

where W_L^\pm denote the $SU(2)_L$ gauge bosons, and $\tan \beta \equiv v_d/v_u$. The mass matrix is diagonalized with an orthogonal matrix:

$$\begin{pmatrix} W_L^+ \\ W_R^+ \end{pmatrix} = \begin{pmatrix} \cos \phi_{LR}^W & -\sin \phi_{LR}^W \\ \sin \phi_{LR}^W & \cos \phi_{LR}^W \end{pmatrix} \begin{pmatrix} W_1^+ \\ W_2^+ \end{pmatrix}. \quad (15)$$

Here, W_1^+ and W_2^+ are the mass eigenstates of the charged gauge bosons. The corresponding eigenvalues are m_W and m_{W_R} , respectively, with $m_W \simeq g_L v/\sqrt{2}$ and m_{W_R} given by Eq. (10). In what follows, we refer to the $SU(2)_L$ -gauge-boson-like state W_1^+ as W^+ . Since the mixing angle ϕ_{LR}^W turns out to be extremely small in our scenario, we denote W_2^+ also by W_R^+ unless otherwise noted. The mixing angle ϕ_{LR}^W is then given by

$$\tan 2\phi_{LR}^W = \frac{2g_L g_R v^2 \sin 2\beta}{g_R^2 v_R^2 - (g_L^2 - g_R^2)v^2} \simeq 2 \sin 2\beta \left(\frac{g_R}{g_L}\right) \frac{m_W^2}{m_{W_R}^2}. \quad (16)$$

The couplings of W and W_R to fermions are given as follows:

$$\begin{aligned} \mathcal{L}_{W_R f f} = & \frac{g_L}{\sqrt{2}} \bar{u} (\cos \phi_{LR}^W W^+ - \sin \phi_{LR}^W W_R^+) P_L d + \frac{g_R}{\sqrt{2}} \bar{u} (\sin \phi_{LR}^W W^+ + \cos \phi_{LR}^W W_R^+) P_R d \\ & + \frac{g_L}{\sqrt{2}} \bar{\nu} (\cos \phi_{LR}^W W^+ - \sin \phi_{LR}^W W_R^+) P_L e + \frac{g_R}{\sqrt{2}} \bar{N}_1 (\sin \phi_{LR}^W W^+ + \cos \phi_{LR}^W W_R^+) P_R e \\ & + \text{h.c.} , \end{aligned} \quad (17)$$

where we suppress the flavor indices for simplicity. In the mass eigenbasis, the W_R - W - Z interaction is given by

$$\begin{aligned} \mathcal{L}_{W_R W Z} = & -ig_Z \sin \phi_{LR}^W \cos \phi_{LR}^W (W_{\mu\nu}^+ W_R^{-\mu} + W_{R\mu\nu}^+ W^{-\mu} - W_{\mu\nu}^- W_R^{+\mu} - W_{R\mu\nu}^- W^{+\mu}) Z^\nu \\ & - ig_Z \sin \phi_{LR}^W \cos \phi_{LR}^W (W_\mu^+ W_{R\nu}^- + W_{R\mu}^+ W_\nu^-) Z^{\mu\nu} , \end{aligned} \quad (18)$$

where $V_{\mu\nu} \equiv \partial_\mu V_\nu - \partial_\nu V_\mu$ ($V = W, W_R$, or Z) and $g_Z \equiv \sqrt{g'^2 + g_L^2}$. As for the $W_R W h$ coupling, we have

$$\mathcal{L}_{W_R W h} = -\frac{1}{2\sqrt{2}} [(g_L^2 - g_R^2) \sin 2\phi_{LR}^W + 2g_L g_R \sin 2\beta \cos 2\phi_{LR}^W] v h (W^- W_R^+ + W_R^- W^+) . \quad (19)$$

Now we evaluate the partial decay widths of W_R . For the fermion channels, $W_R \rightarrow f \bar{f}'$, we have

$$\Gamma(W_R^+ \rightarrow u \bar{d}) = \Gamma(W_R^+ \rightarrow c \bar{s}) = \frac{g_R^2}{16\pi} m_{W_R} , \quad (20)$$

$$\Gamma(W_R^+ \rightarrow t \bar{b}) = \frac{g_R^2}{16\pi} m_{W_R} \left(1 + \frac{m_t^2}{2m_{W_R}^2} \right) \left(1 - \frac{m_t^2}{m_{W_R}^2} \right)^2 , \quad (21)$$

$$\Gamma(W_R^+ \rightarrow N_1 \bar{e}) = \frac{g_R^2}{48\pi} m_{W_R} \left(1 + \frac{m_{N_1}^2}{2m_{W_R}^2} \right) \left(1 - \frac{m_{N_1}^2}{m_{W_R}^2} \right)^2 , \quad (22)$$

where we have neglected the small mixing factor ϕ_{LR}^W . For the $W_R \rightarrow W Z$ decay process, we have

$$\begin{aligned} \Gamma(W_R^+ \rightarrow W^+ Z) = & \frac{g_R^2}{192\pi} \sin^2(2\beta) m_{W_R} \left(1 - 2 \frac{m_W^2 + m_Z^2}{m_{W_R}^2} + \frac{(m_W^2 - m_Z^2)^2}{m_{W_R}^4} \right)^{\frac{3}{2}} \\ & \times \left(1 + 10 \frac{m_W^2 + m_Z^2}{m_{W_R}^2} + \frac{m_{W_R}^4 + 10m_W^2 m_Z^2 + m_Z^4}{m_{W_R}^4} \right) . \end{aligned} \quad (23)$$

Here, notice that although the W_R - W - Z coupling in Eq. (18) is suppressed by the small mixing angle ϕ_{LR}^W , the partial decay width of the $W Z$ channel does not suffer from this suppression. This is because the high-energy behavior of the longitudinal mode of W_R gives an enhancement factor of $\sim (m_{W_R}/m_W)^4$ and this compensates the suppression factor from the mixing angle. Finally, the $W_R \rightarrow W h$ decay width is given by

$$\begin{aligned} \Gamma(W_R^+ \rightarrow W^+ h) = & \frac{g_R^2}{192\pi} \sin^2(2\beta) m_{W_R} \left(1 - 2 \frac{m_W^2 + m_h^2}{m_{W_R}^2} + \frac{(m_W^2 - m_h^2)^2}{m_{W_R}^4} \right)^{\frac{1}{2}} \\ & \times \left(1 + \frac{10m_W^2 - 2m_h^2}{m_{W_R}^2} + \frac{(m_W^2 - m_h^2)^2}{m_{W_R}^4} \right) , \end{aligned} \quad (24)$$

where we assume the decoupling limit for the Higgs bosons in our model. Notice that in the large m_{W_R} limit,

$$\Gamma(W_R^+ \rightarrow W^+ Z) \simeq \Gamma(W_R^+ \rightarrow W^+ h) , \quad (25)$$

holds. This is a consequence of the equivalence theorem.

As seen above, the lightest Dirac neutrino N_1 is generated as a decay product of W_R . The decay branching ratios of N_1 highly depend on its mass and the left-right mixing in both the gauge boson and neutrino sectors. When the mass of N_1 is rather large and the left-right mixing is very small, the three-body decay process via the virtual W_R^+ exchange is dominant. The three-body decay width into an electron plus a pair of the first/second generation quarks is given by [4]

$$\Gamma(N_1 \rightarrow \bar{q}q'e^-) = \frac{g_R^4}{2048\pi^3} m_{N_1} F(x) , \quad (26)$$

with $x = m_{N_1}^2/m_{W_R}^2$ and

$$F(x) = \frac{12}{x} \left[1 - \frac{x}{2} - \frac{x^2}{6} + \frac{1-x}{x} \ln(1-x) \right] . \quad (27)$$

Here we neglect the quark and electron masses. For the $N_1 \rightarrow \bar{b}te^-$ decay channel, we have [9]

$$\Gamma(N_1 \rightarrow \bar{b}te^-) = \frac{g_R^4}{2048\pi^3} m_{N_1} F_t(x, y) , \quad (28)$$

where

$$\begin{aligned} F_t(x, y) = & \frac{12}{x} \left[(1-y) - \frac{x}{2}(1-y^2) - \frac{x^2}{6} \left(1 - \frac{3}{2}y + \frac{3}{2}y^2 - y^3 \right) \right. \\ & - \frac{5x^3y}{8}(1-y^2) + \frac{x^4y^2(1-y)}{4} - \frac{x^3y^2}{4}(4+x^2y) \ln y \\ & \left. + \frac{1-x}{x} \ln \left(\frac{1-x}{1-xy} \right) \left\{ 1 - \frac{xy}{4} [4+x+x^2-x^3y^2(1+x)] \right\} \right] , \quad (29) \end{aligned}$$

with $y \equiv m_t^2/m_{N_1}^2$ (m_t is the top mass). Of course, $F_t(x, y) \rightarrow F(x)$ as $y \rightarrow 0$. We note in passing that the functions $F(x)$ and $F_t(x, y)$ also appear in the calculation of the muon decay width [35].

On the other hand, if m_{N_1} is relatively small and if ϕ_{LR}^W or the mixing of N_1 with left-handed neutrinos ν_l , \mathcal{R}_{l1} , is sizable, then the two-body decay processes become dominant. In what follows, we assume that only the \mathcal{R}_{e1} component can be sizable and the other flavor off-diagonal components, $\mathcal{R}_{\mu 1}$ and $\mathcal{R}_{\tau 1}$, are always negligible for simplicity.⁴ The

⁴We here note that this assumption is consistent with the experimental data of neutrino oscillations, as discussed in Ref. [25].

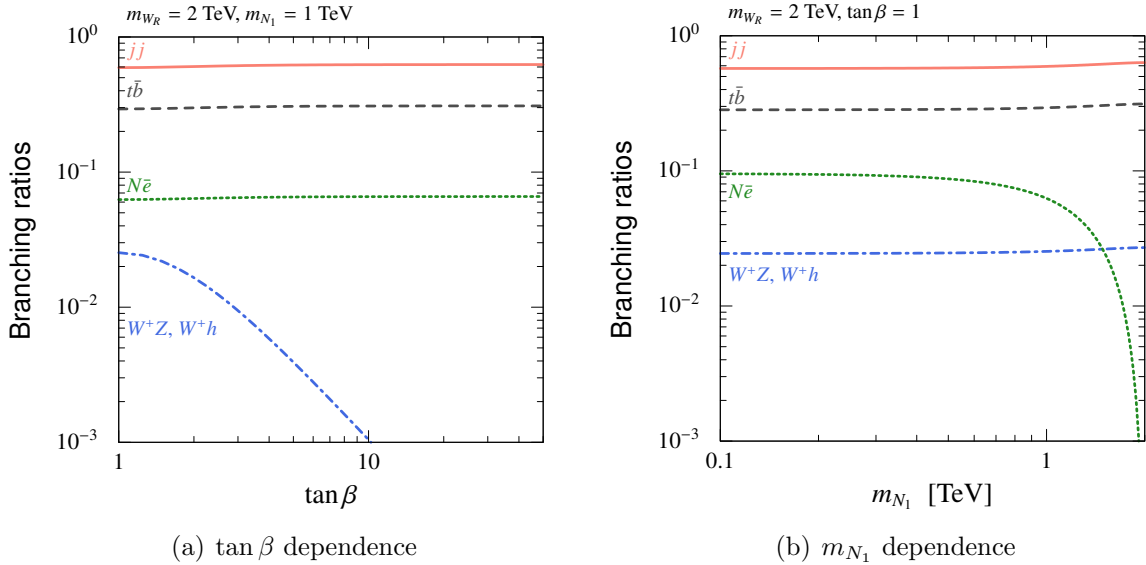


Figure 2: Branching ratios of the W_R^+ decay as functions of $\tan\beta$ and m_{N_1} in Figs. 2(a) and 2(b), respectively. Here, we set $m_{W_R} = 2$ TeV. The red solid, black dashed, green dotted, and blue dash-dotted lines represent the branching fractions of the dijet, $t\bar{b}$, $N_1 e^+$, and W^+Z and W^+h channels, respectively. m_{N_1} is fixed to be 1 TeV in Fig. 2(a), while $\tan\beta = 1$ in Fig. 2(b).

relevant partial decay widths are then given as follows:

$$\Gamma(N_1 \rightarrow e^- W^+) = \frac{g_L^2 |\mathcal{R}_{e1}|^2 + g_R^2 \sin^2 \phi_{LR}^W m_{N_1}^3}{64\pi m_W^2} \left(1 - \frac{m_W^2}{m_{N_1}^2}\right)^2 \left(1 + 2 \frac{m_W^2}{m_{N_1}^2}\right), \quad (30)$$

$$\Gamma(N_1 \rightarrow \nu_e Z) = \frac{g_Z^2 |\mathcal{R}_{e1}|^2 m_{N_1}^3}{128\pi m_Z^2} \left(1 - \frac{m_Z^2}{m_{N_1}^2}\right)^2 \left(1 + 2 \frac{m_Z^2}{m_{N_1}^2}\right), \quad (31)$$

$$\Gamma(N_1 \rightarrow \nu_e h) = \frac{g_L^2 |\mathcal{R}_{e1}|^2 m_{N_1}^3}{128\pi m_W^2} \left(1 - \frac{m_h^2}{m_{N_1}^2}\right)^2. \quad (32)$$

By using the above formulae, we now evaluate the decay branching fractions of W_R and N_1 . First, we show the branching ratios of the W_R^+ decay as functions of $\tan\beta$ and m_{N_1} in Figs. 2(a) and 2(b), respectively. Here, we set $m_{W_R} = 2$ TeV. The red solid, black dashed, green dotted, and blue dash-dotted lines represent the branching fractions of the dijet, $t\bar{b}$, $N_1 e^+$, and W^+Z and W^+h channels, respectively. m_{N_1} is fixed to be 1 TeV in Fig. 2(a), while $\tan\beta = 1$ in Fig. 2(b). From these figures, we find that about 10% of W_R decay into a pair of N_1 and e^+ when $m_{N_1} \lesssim 1$ TeV. This decay branch hardly depends on $\tan\beta$. Such a sizable decay fraction allows the model to explain the CMS $eejj$ excess, as we will see below. The decay branch of WZ channel, on the other hand, strongly depends on $\tan\beta$. In particular, this model can explain the ATLAS diboson anomaly [12] only if $\tan\beta$ is small; otherwise, the diboson decay mode is almost negligible.

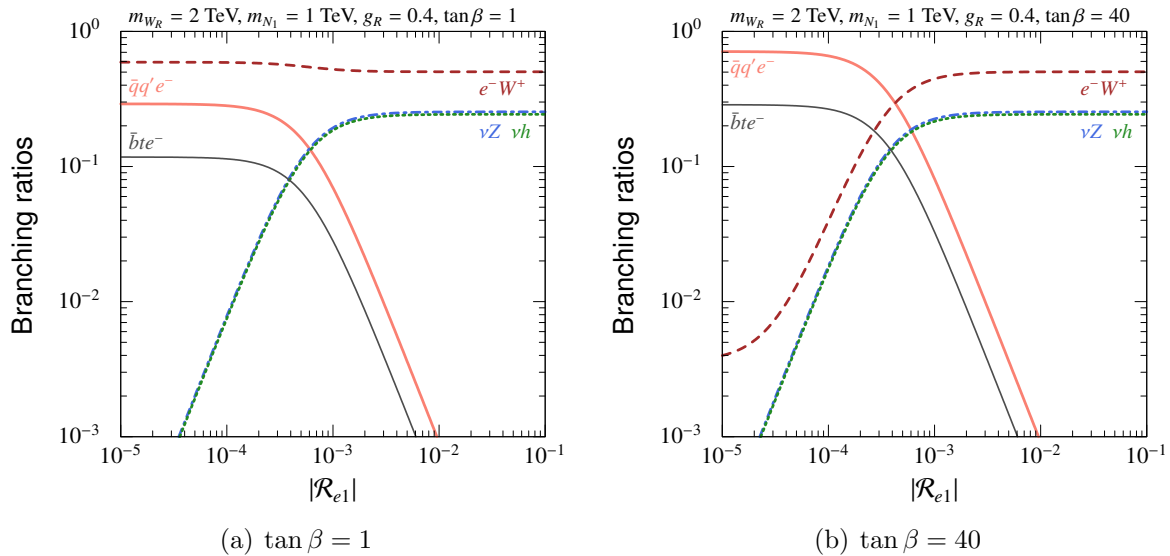


Figure 3: Branching ratios of the N_1 decay as functions of $|\mathcal{R}_{e1}|$. Here, we set $m_{W_R} = 2$ TeV, $m_{N_1} = 1$ TeV, and $g_R = 0.4$. The red bold, black thin, brown dashed, green dotted, and blue dash-dotted lines represent the branching fractions of the $\bar{q}q'e^-$, $\bar{b}te^-$, e^-W^+ , νZ , and νh channels, respectively.

Next, we evaluate the decay fractions of N_1 . We plot the branching ratios of the N_1 decay as functions of $|\mathcal{R}_{e1}|$ and m_{N_1} in Figs. 3 and 4, respectively. Here, we set $m_{W_R} = 2$ TeV and $g_R = 0.4$. The red bold, black thin, brown dashed, green dotted, and blue dash-dotted lines represent the branching fractions of the $\bar{q}q'e^-$, $\bar{b}te^-$, e^-W^+ , νZ , and νh channels, respectively. m_{N_1} is fixed to be 1 TeV in Fig. 3, while $|\mathcal{R}_{e1}| = 0.001$ in Fig. 4. From Fig. 3, we find that the three-body channels are sizable only when $|\mathcal{R}_{e1}|$ is rather small. When $|\mathcal{R}_{e1}|$ is large, the two-body decay channels become dominant as they are induced via the left-right mixing in the neutrino sector in this case. However, even in the small $|\mathcal{R}_{e1}|$ region, the branching fraction of the e^-W^+ decay channel can still be sizable, depending on the value of $\tan\beta$; this is because in this region the e^-W^+ decay is induced by the $W-W_R$ mixing. As we see in Sec. 4.1, $\tan\beta \simeq 1$ is favored in order to explain the ATLAS diboson anomaly. In this case, the e^-W^+ channel is the dominant decay mode for any value of $|\mathcal{R}_{e1}|$, as can be seen from Fig. 3(a). This allows us to test our model with the trilepton plus missing energy channel. On the other hand, Fig. 4 shows that the branching fractions of the three-body channels significantly depend on the mass of the right-handed neutrino, while those of the two-body channels have relatively small dependence on m_{N_1} .

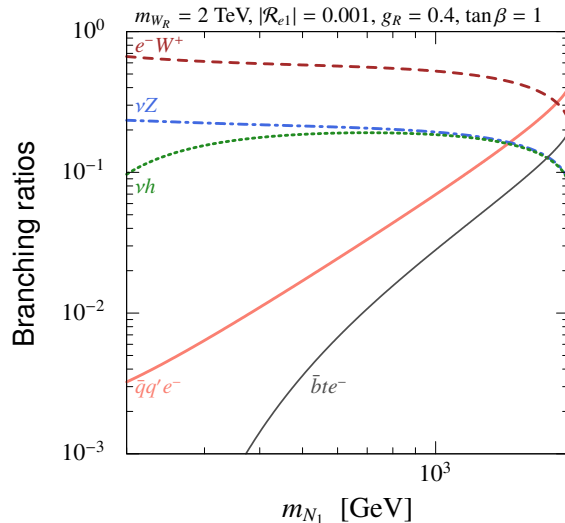


Figure 4: Branching ratios of the N_1 decay as functions of m_{N_1} . Here, we set $m_{W_R} = 2$ TeV, $|\mathcal{R}_{e1}| = 0.001$, $g_R = 0.4$, and $\tan\beta = 1$. The red bold, black thin, brown dashed, green dotted, and blue dash-dotted lines represent the branching fractions of the $\bar{q}q'e^-$, $\bar{b}te^-$, e^-W^+ , νZ , and νh channels, respectively.

4 LHC Signatures

Now we study the LHC signature of our model. First, in Sec. 4.1, we show the favored parameter space to explain the excess events observed by the ATLAS collaboration in their diboson resonance search [12]. Next, we consider the $eejj$ channel and determine the parameters with which the model can explain the excess events observed by the CMS collaboration [1]. Then, in Sec. 4.3, we discuss prospects for probing our model by using the trilepton plus missing energy searches.

4.1 Diboson resonance search

The ATLAS collaboration has recently announced excessive events in the diboson resonance search using fully hadronic decay channel [12]. In this case, each gauge boson is reconstructed as a fat jet since a gauge boson coming from a heavy resonance is highly boosted so that the final-state two quarks from the gauge boson are observed as a single large-radius jet. The ATLAS collaboration has observed a narrow resonance around 2 TeV in the invariant mass distributions of two fat jets, with its local significance of 3.4σ in the WZ channel. The CMS collaboration also found a small excess around 1.9 TeV [36] in a similar analysis. Recently, the ATLAS collaboration [37] combined the results of searches for diboson resonances decaying into leptonic [38], semi-leptonic [39, 40], and hadronic final states [12], and still found a 2.5σ deviation from the SM prediction. Taking into account these results, as well as those from the CMS semileptonic search [41], the authors in Ref. [42] have found that the above results are well fitted with a 2 TeV W_R

whose production cross section, $\sigma(pp \rightarrow W_R)$, times the branching fraction of the WZ decay channel, $\text{BR}(W_R \rightarrow WZ)$, is

$$\sigma(pp \rightarrow W_R) \times \text{BR}(W_R \rightarrow WZ) = 4.3_{-1.5}^{+2.1} \text{ fb} . \quad (33)$$

We further note that the 13 TeV diboson resonance searches from both the ATLAS [43] and CMS [44] collaborations are found to be still too weak to constrain these possible anomalies observed at the LHC Run-I.

Let us see if our model can reproduce the required value of $\sigma(pp \rightarrow W_R) \times \text{BR}(W_R \rightarrow WZ)$ given in Eq. (33). We compute the production cross section of a 2 TeV W_R at $\sqrt{s} = 8$ TeV by using MadGraph5 [45] as

$$\sigma(pp \rightarrow W_R) \simeq 90 \times \left(\frac{g_R}{0.4}\right)^2 \text{ fb} . \quad (34)$$

Here, we re-scale the cross section by the so-called k factor, $k \simeq 1.3$ [46, 47], to include the effects of the higher-order QCD corrections. To obtain the value in Eq. (33), therefore, we need

$$\text{BR}(W_R \rightarrow WZ) = 4.8_{-1.7}^{+2.3} \times 10^{-2} , \quad (35)$$

for $m_{W_R} = 2$ TeV and $g_R = 0.4$. From Fig. 2, we find that this model can explain a part of the diboson excess only if $\tan\beta \simeq 1$. This observation motivates us to consider the $\tan\beta \simeq 1$ case. In this case, the left-right mixing in the gauge boson sector is sizable, which plays an important role in the phenomenology of the N_1 decay as we have seen in the previous section.

Although our setup discussed here predicts a smaller number of events in the diboson channel than the observed one, our model still may explain all of the events with the W_R . For instance, by enhancing the production cross section of W_R , we may increase the number of events. This can be realized if we consider a slightly lighter W_R (note that we cannot enhance the production cross section by using a larger value of g_R as it predicts a too light Z_R , as can be seen from Fig. 1); for example, we obtain $\sigma(pp \rightarrow W_R) \simeq 130$ fb for $m_{W_R} = 1.9$ TeV and $g_R = 0.4$. On the other hand, for a 1.9 TeV W_R , $\sigma(pp \rightarrow W_R) \times \text{BR}(W_R \rightarrow WZ) = 5.3_{-2.0}^{+2.3}$ fb is favored from the experiments according to Ref. [42]. This means $\text{BR}(W_R \rightarrow WZ) = 4.1_{-1.5}^{+1.9} \times 10^{-2}$, which is relatively close to the model prediction for $\tan\beta = 1$. Another way is to introduce an extra Higgs field, *e.g.*, an $\text{SU}(2)_R$ triplet Higgs field, which gives an additional contribution to the Z_R mass. In this case, we may take a larger value of g_R with keeping m_{Z_R} large enough. By taking the couplings of the additional Higgs field with the fermions in our model (especially with right-handed neutrinos) sufficiently small, we can keep heavy neutrinos pseudo-Dirac. Anyway, given the small statistics at present, it is unclear whether our model can explain the diboson anomaly without going beyond the minimal setup or not. This situation should be settled by the LHC Run-II experiments in the near future.

There are several other decay channels which may constrain a 2 TeV W_R . Figure 2 shows that W_R mainly decays into light quarks, and thus dijet resonance searches can give a strong limit on the production of W_R . At present, the ATLAS dijet resonance

search based on the 3.6 fb^{-1} data at the 13 TeV run gives the severest limit [48]: $\sigma(pp \rightarrow W_R) \times \mathcal{A} \times \text{BR}(W_R \rightarrow jj) \lesssim 180 \text{ fb}$ with $\mathcal{A} \simeq 0.4$ being the acceptance. The CMS limit is less severe than the ATLAS one because of the smaller number of integrated luminosity [49]. On the other hand, the production cross section of a W_R at $\sqrt{s} = 13 \text{ TeV}$ is evaluated as $\sigma(pp \rightarrow W_R) \simeq 557 \text{ fb}$ for $m_{W_R} = 2 \text{ TeV}$ and $g_R = 0.4$. Here, we have used the k -factor of $k = 1.2$ [46, 47]. Hence, the present ATLAS bound [48] reads $\text{BR}(W_R \rightarrow jj) \lesssim 0.81$, which is satisfied in our model as can be seen from Fig. 2. The third-generation-quark resonance search can also restrict this model. The strongest limit is currently given by the CMS collaboration based on the 8 TeV run [50]: $\sigma(pp \rightarrow W_R) \times \text{BR}(W_R \rightarrow tb) \lesssim 40 \text{ fb}$ for a 2 TeV W_R , which leads to $\text{BR}(W_R \rightarrow tb) \lesssim 0.44$ for $g_R = 0.4$. Our model prediction is $\text{BR}(W_R \rightarrow tb) \simeq 0.3$, which is below the present limit.

Finally, we comment on the indirect limit on the W - W_R mixing from the electroweak precision measurements. As seen above, to explain the ATLAS diboson anomaly in our model, $\tan\beta \simeq 1$ is required, which implies that the W - W_R mixing angle should be $\mathcal{O}(10^{-3})$. This size of the W - W_R mixing potentially conflicts with the electroweak precision measurements. Here, note that we cannot use the S and T parameters [51] to assess the consistency of our model with the electroweak precision measurements, since our model also contains a Z_R and it modifies the Z -boson coupling to the SM fermions at tree level through the Z - Z_R mixing. Instead, we need to carry out a complete parameter fitting onto the electroweak observables. Such a parameter fitting is done in Refs. [46, 52] and it is found that a 2 TeV W_R with an $\mathcal{O}(10^{-3})$ W - W_R mixing is actually consistent with the electroweak precision experiments.

4.2 $eejj$ Channel

Next, we discuss the $eejj$ channel. The CMS collaboration has observed a 2.8σ anomaly in this channel [1] with the 19.7 fb^{-1} 8 TeV data, which also indicates the presence of W_R with a mass of around 2 TeV. 14 events are observed around 2 TeV, while 4 events are expected from the SM backgrounds. Among the 14 events, only one event consists of same-sign dielectron, while the rest of 13 events include opposite-sign electrons. The number of the same-sign dielectron events due to the SM backgrounds is expected to be $\mathcal{O}(0.5)$; thus, this observation is totally consistent with a hypothesis that all of the signal events consist of opposite-sign dielectron events. The signal acceptance \mathcal{A} is listed in Ref. [1]; for instance, for $m_{W_R} = 2 \text{ TeV}$ and $m_{N_1} = 1 \text{ TeV}$, we have $\mathcal{A} = 0.784 \pm 0.009$. This implies that if the signal cross section of the $eejj$ channel is $\simeq 0.65 \text{ fb}$, then the predicted number of events falls right in the middle of the observed number.

In our model, the $eejj$ decay process is induced via the virtual W_R exchange by a N_1 ,

$$W_R \rightarrow eN_1 \rightarrow eeW_R^* \rightarrow eejj , \quad (36)$$

as well as via the on-shell W which is a decay product of N_1 :

$$W_R \rightarrow eN_1 \rightarrow eeW \rightarrow eejj . \quad (37)$$

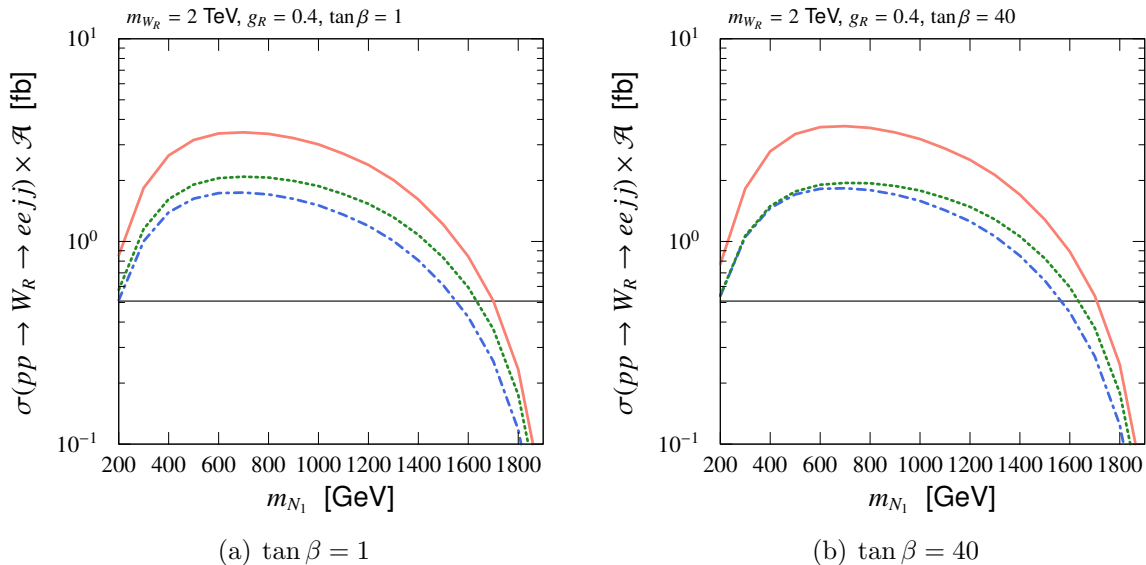


Figure 5: Signal cross section for the $eejj$ channel times the acceptance \mathcal{A} as functions of m_{N_1} . Here, we set $m_{W_R} = 2$ TeV and $g_R = 0.4$. The red solid, green dotted, and blue dash-dotted lines show the cases of $|\mathcal{R}_{e1}| = 10^{-4}$, 10^{-3} , and 10^{-2} , respectively. The horizontal gray line corresponds to 10 events for an integrated luminosity of 19.7 fb^{-1} .

Notice that we expect opposite-sign electrons in the final state, rather than same-sign dielectron, since lepton-number violation is significantly suppressed by the very small mass parameters μ_{ij} in our model. This is consistent with the CMS observation.

In Fig. 5, we plot the signal cross section for the $eejj$ channel times the acceptance \mathcal{A} as functions of m_{N_1} . Here, we set $m_{W_R} = 2$ TeV and $g_R = 0.4$. The red solid, green dotted, and blue dash-dotted lines show the cases of $|\mathcal{R}_{e1}| = 10^{-4}$, 10^{-3} , and 10^{-2} , respectively. The acceptance is taken from Ref. [1]. From these plots, we find that although the decay branching ratios of N_1 significantly depend on $\tan\beta$ as shown in Fig. 3, the signal cross section for the $eejj$ mode does not depend on $\tan\beta$ so much; if one takes $\tan\beta$ large, the eW decay channel of N_1 could be subdominant, but in this case the three-body $eejj$ decay mode becomes dominant, which makes the total signal cross section for the $eejj$ decay channel almost unchanged. We also show the value of the signal cross section which corresponds to 10 events for an integrated luminosity of 19.7 fb^{-1} by the horizontal gray line in this figure. It is found that the observed event number is reproduced if m_{N_1} is in the range of $\sim 1.5\text{--}1.7$ TeV. We however note that because of the low statistics we expect a large uncertainty in the extraction of the favored signal cross section. Furthermore, our computation also suffers from uncertainty resulting from the estimation of the acceptance. In our analysis, we took the acceptance rate given by the CMS collaboration [1]. However, this acceptance is estimated for the three-body decay of N_1 via the off-shell W_R exchange process. On the other hand, in our model, the two-body decay of N_1 into eW also gives rise to the $eejj$ final state. This contribution may result in a different value of acceptance

A. Considering these possible uncertainties, we conclude that at present any values of $m_{N_1} \sim 1$ TeV may be consistent with the CMS $eejj$ search result.

4.3 Trilepton Channel

Now let us discuss possibilities to probe our model in the trilepton plus large missing energy mode. As we have seen in Sec. 4.1, $\tan\beta \simeq 1$ is favored in order to explain the ATLAS diboson anomaly. In this case, the dominant decay mode of N_1 is always the eW final state. This state can subsequently decay into the three charged leptons plus a light neutrino final state. Therefore, our setup discussed so far in general predicts a sizable signal rate in the trilepton plus large missing energy searches.

To illustrate this, we compare the prediction of our model with the CMS result of the search for the trilepton plus missing energy signatures at the center-of-mass energy of $\sqrt{s} = 8$ TeV with the 19.5 fb^{-1} integrated luminosity [28]. As we have assumed above, the flavor-violating processes are negligible in our setup. Hence, we focus on events which contain an opposite-sign same-flavor (OSSF) lepton pair. This category is called OSSF1 in Ref. [28]. Moreover, since N_1 only couples to an electron, this pair should be e^+e^- .⁵ Therefore, the trilepton events we consider below include either $e^+e^-e^\pm$ or $e^+e^-\mu^\pm$.

In our analysis, we generate the trilepton plus missing energy events using `MadGraph5` [45] and evaluate the parton-level cross sections with the `CTEQ6L` parton distribution function set [53]. The cross sections are multiplied by the k -factor of $k = 1.3$ [46, 47]. The showering and hadronization are executed with `PYTHIA6.4` [54], while we use `DELPHES3` [55] for the detector simulation. Jet-clustering is performed with `FastJet2` [56] based on the anti- k_T algorithm with a distance parameter of 0.5. We impose the same criterion for the event selection as those used in Ref. [28]:

- Electrons and muons are required to satisfy that their transverse momentum p_T be larger than 10 GeV and the magnitude of their pseudo-rapidity η be smaller than 2.4. They should be separated from each other by $\Delta R \equiv \sqrt{(\Delta\eta)^2 + (\Delta\phi)^2} > 0.1$, where ϕ is the azimuthal angle.
- At least one electron or muon should have $p_T > 20$ GeV.
- Jets should satisfy $p_T > 30$ GeV and $|\eta| < 2.5$. They are required to be separated from a lepton by $\Delta R > 0.3$.
- For each event, we construct OSSF charged leptons $\ell^+\ell^-$ ($\ell = e, \mu$) and require that the invariant mass of these charged leptons, $m_{\ell^+\ell^-}$, should be ≥ 12 GeV.
- We reject the “on- Z ” events in which a pair of OSSF charged leptons yields $75 < m_{\ell^+\ell^-} < 105$ GeV.

⁵As we will state soon below, we veto events if the invariant mass of any pair of OSSF charged leptons is reconstructed to be around the Z -boson mass. This rejects the $N_1 \rightarrow \nu Z$ events, and thus we do not expect final states which include a pair of $\mu^+\mu^-$.

Table 1: Simulated number of events in our model for the 8 TeV run with an integrated luminosity of 19.5 fb^{-1} . Here, we set $m_{W_R} = 2 \text{ TeV}$, $g_R = 0.4$, $\mathcal{R}_{e1} = 10^{-3}$, and $\tan \beta = 1$.

| Category | $m_{\ell+\ell-}$ | $m_{N_1} = 1 \text{ TeV}$ | 1.6 TeV | Observed | Expected |
|--|------------------|---------------------------|---------|----------|----------------|
| $H_T > 200 \text{ GeV}$ | | | | | |
| $E_T^{\text{miss}} > 100 \text{ GeV}$ | Above-Z | 1.86 | 0.85 | 5 | 3.6 ± 1.2 |
| | Below-Z | 0 | 0 | 7 | 9.7 ± 3.3 |
| $50 < E_T^{\text{miss}} < 100 \text{ GeV}$ | Above-Z | 0.22 | 0.02 | 4 | 5.0 ± 1.6 |
| | Below-Z | 0 | 0 | 10 | 11.0 ± 3.8 |
| $E_T^{\text{miss}} < 50 \text{ GeV}$ | Above-Z | 0 | 0 | 3 | 7.3 ± 2.0 |
| | Below-Z | 0 | 0 | 26 | 25.0 ± 6.8 |
| $H_T < 200 \text{ GeV}$ | | | | | |
| $E_T^{\text{miss}} > 100 \text{ GeV}$ | Above-Z | 2.01 | 0.92 | 18 | 13.0 ± 3.5 |
| | Below-Z | 0.13 | 0 | 21 | 24 ± 9 |
| $50 < E_T^{\text{miss}} < 100 \text{ GeV}$ | Above-Z | 0.14 | 0 | 50 | 46.0 ± 9.7 |
| | Below-Z | 0 | 0 | 142 | 130 ± 27 |
| $E_T^{\text{miss}} < 50 \text{ GeV}$ | Above-Z | 0.16 | 0 | 178 | 200 ± 35 |
| | Below-Z | 0 | 0 | 510 | 560 ± 87 |

Then, we classify each event into several categories according to Ref. [28]. Firstly, we divide all events into two classes: one with the scalar sum of jet transverse momentum, H_T , being $H_T > 200 \text{ GeV}$ and the other with $H_T < 200 \text{ GeV}$. Secondly, we divide each class in terms of the missing transverse energy E_T^{miss} : $E_T^{\text{miss}} > 100 \text{ GeV}$, $50 < E_T^{\text{miss}} < 100 \text{ GeV}$, or $E_T^{\text{miss}} < 50 \text{ GeV}$. Here, E_T^{miss} is the magnitude of the vector sum of the transverse momenta. Finally, if all possible OSSF pairs give $m_{\ell+\ell-} > 105 \text{ GeV}$ ($m_{\ell+\ell-} < 75 \text{ GeV}$), then the corresponding event is called an above-Z (below-Z) event.

In Table 1 and 2, we show the number of events in each category simulated in our analysis for the 8 TeV run with an integrated luminosity of 19.5 fb^{-1} . Here, we set $m_{W_R} = 2 \text{ TeV}$, $g_R = 0.4$, $\tan \beta = 1$ and $\mathcal{R}_{e1} = 10^{-3}$ ($\mathcal{R}_{e1} = 10^{-5}$) in Table 1 (Table 2). We show the results for two cases, $m_{N_1} = 1$ and 1.6 TeV. It turns out that our model prediction is consistent with the current data. Moreover, we find that our model potentially accounts for a small deviation from the SM prediction in the $H_T < 200 \text{ GeV}$, $E_T^{\text{miss}} > 100 \text{ GeV}$, and $m_{\ell+\ell-} > 105 \text{ GeV}$ category without conflicting with the results in the other categories. This observation indicates that the trilepton plus missing energy search at the LHC Run-II will offer a promising way to test our scenario in the near future, together with other W_R searches.

Table 2: Simulated number of events in our model for the 8 TeV run with an integrated luminosity of 19.5 fb^{-1} . Here, we set $m_{W_R} = 2 \text{ TeV}$, $g_R = 0.4$, $\mathcal{R}_{e1} = 10^{-5}$, and $\tan \beta = 1$.

| Category | $m_{\ell+\ell^-}$ | $m_{N_1} = 1 \text{ TeV}$ | 1.6 TeV | Observed | Expected |
|--|-------------------|---------------------------|---------|----------|----------------|
| $H_T > 200 \text{ GeV}$ | | | | | |
| $E_T^{\text{miss}} > 100 \text{ GeV}$ | Above-Z | 4.76 | 1.67 | 5 | 3.6 ± 1.2 |
| | Below-Z | 0 | 0 | 7 | 9.7 ± 3.3 |
| $50 < E_T^{\text{miss}} < 100 \text{ GeV}$ | Above-Z | 0.60 | 0.03 | 4 | 5.0 ± 1.6 |
| | Below-Z | 0 | 0 | 10 | 11.0 ± 3.8 |
| $E_T^{\text{miss}} < 50 \text{ GeV}$ | Above-Z | 0 | 0 | 3 | 7.3 ± 2.0 |
| | Below-Z | 0 | 0 | 26 | 25.0 ± 6.8 |
| $H_T < 200 \text{ GeV}$ | | | | | |
| $E_T^{\text{miss}} > 100 \text{ GeV}$ | Above-Z | 5.53 | 1.81 | 18 | 13.0 ± 3.5 |
| | Below-Z | 0.38 | 0 | 21 | 24 ± 9 |
| $50 < E_T^{\text{miss}} < 100 \text{ GeV}$ | Above-Z | 0.44 | 0 | 50 | 46.0 ± 9.7 |
| | Below-Z | 0 | 0 | 142 | 130 ± 27 |
| $E_T^{\text{miss}} < 50 \text{ GeV}$ | Above-Z | 0.47 | 0 | 178 | 200 ± 35 |
| | Below-Z | 0 | 0 | 510 | 560 ± 87 |

5 Conclusion and Discussions

In this paper, we have discussed an extended gauge sector model based on the $SU(2)_L \otimes SU(2)_R \otimes U(1)_{B-L}$ gauge theory which accommodates the inverse seesaw structure in the neutrino sector. We have found that our model can explain the CMS $eejj$ anomaly and the ATLAS diboson excess simultaneously, without conflicting with existing experimental bounds. To explain these two anomalies, we need sizable left-right mixing in the gauge sector. Such left-right mixing can also appear in the neutrino sector because of the inverse seesaw structure. This allows us to probe our model in the searches for the trilepton plus missing energy signatures. After all, we expect that the LHC Run-II experiments will test our setup in the near future and shed light on the nature of TeV-scale physics beyond the SM.

Acknowledgments

The work of N.N. was supported by DOE grant No. DE-SC0011842 at the University of Minnesota. The work of N.O. was supported by DOE grant No. DE-SC0013680.

References

- [1] V. Khachatryan *et al.* [CMS Collaboration], *Eur. Phys. J. C* **74**, no. 11, 3149 (2014) [arXiv:1407.3683 [hep-ex]].
- [2] Y. Bai and J. Berger, *Phys. Lett. B* **746**, 32 (2015) [arXiv:1407.4466 [hep-ph]]; B. A. Dobrescu and A. Martin, *Phys. Rev. D* **91**, no. 3, 035019 (2015) [arXiv:1408.1082 [hep-ph]]; B. Allanach, S. Biswas, S. Mondal and M. Mitra, *Phys. Rev. D* **91**, no. 1, 011702 (2015) [arXiv:1408.5439 [hep-ph]]; S. Biswas, D. Chowdhury, S. Han and S. J. Lee, *JHEP* **1502**, 142 (2015) [arXiv:1409.0882 [hep-ph]]; B. C. Allanach, S. Biswas, S. Mondal and M. Mitra, *Phys. Rev. D* **91**, no. 1, 015011 (2015) [arXiv:1410.5947 [hep-ph]]; M. Dhuria, C. Hati, R. Rangarajan and U. Sarkar, *Phys. Rev. D* **91**, no. 5, 055010 (2015) [arXiv:1501.04815 [hep-ph]]; M. E. Krauss and W. Porod, *Phys. Rev. D* **92**, no. 5, 055019 (2015) [arXiv:1507.04349 [hep-ph]]; M. Dhuria, C. Hati and U. Sarkar, *Phys. Rev. D* **93**, no. 1, 015001 (2016) [arXiv:1507.08297 [hep-ph]].
- [3] F. F. Deppisch, T. E. Gonzalo, S. Patra, N. Sahu and U. Sarkar, *Phys. Rev. D* **90**, no. 5, 053014 (2014) [arXiv:1407.5384 [hep-ph]]; M. Heikinheimo, M. Raidal and C. Spethmann, *Eur. Phys. J. C* **74**, no. 10, 3107 (2014) [arXiv:1407.6908 [hep-ph]]; J. A. Aguilar-Saavedra and F. R. Joaquim, *Phys. Rev. D* **90**, no. 11, 115010 (2014) [arXiv:1408.2456 [hep-ph]]; F. F. Deppisch, T. E. Gonzalo, S. Patra, N. Sahu and U. Sarkar, *Phys. Rev. D* **91**, no. 1, 015018 (2015) [arXiv:1410.6427 [hep-ph]]; P. Coloma, B. A. Dobrescu and J. Lopez-Pavon, *Phys. Rev. D* **92**, no. 11, 115023 (2015) [arXiv:1508.04129 [hep-ph]]; T. Bandyopadhyay, B. Brahmachari and A. Raychaudhuri, arXiv:1509.03232 [hep-ph].
- [4] J. Gluza and T. Jeliski, *Phys. Lett. B* **748**, 125 (2015) [arXiv:1504.05568 [hep-ph]].
- [5] B. A. Dobrescu and Z. Liu, *Phys. Rev. Lett.* **115**, no. 21, 211802 (2015) [arXiv:1506.06736 [hep-ph]].
- [6] P. S. Bhupal Dev and R. N. Mohapatra, *Phys. Rev. Lett.* **115**, no. 18, 181803 (2015) [arXiv:1508.02277 [hep-ph]].
- [7] F. F. Deppisch, L. Graf, S. Kulkarni, S. Patra, W. Rodejohann, N. Sahu and U. Sarkar, *Phys. Rev. D* **93**, no. 1, 013011 (2016) [arXiv:1508.05940 [hep-ph]].
- [8] R. L. Awasthi, P. S. B. Dev and M. Mitra, arXiv:1509.05387 [hep-ph].
- [9] B. A. Dobrescu and P. J. Fox, arXiv:1511.02148 [hep-ph].
- [10] J. C. Pati and A. Salam, *Phys. Rev. D* **10**, 275 (1974) [*Phys. Rev. D* **11**, 703 (1975)]; R. N. Mohapatra and J. C. Pati, *Phys. Rev. D* **11**, 566 (1975); R. N. Mohapatra and J. C. Pati, *Phys. Rev. D* **11**, 2558 (1975); G. Senjanovic and R. N. Mohapatra, *Phys. Rev. D* **12**, 1502 (1975).

- [11] J. Hisano, N. Nagata and Y. Omura, Phys. Rev. D **92**, no. 5, 055001 (2015) [arXiv:1506.03931 [hep-ph]]; K. Cheung, W. Y. Keung, P. Y. Tseng and T. C. Yuan, Phys. Lett. B **751**, 188 (2015) [arXiv:1506.06064 [hep-ph]]; Y. Gao, T. Ghosh, K. Sinha and J. H. Yu, Phys. Rev. D **92**, no. 5, 055030 (2015) [arXiv:1506.07511 [hep-ph]]; J. Brehmer, J. Hewett, J. Kopp, T. Rizzo and J. Tattersall, JHEP **1510**, 182 (2015) [arXiv:1507.00013 [hep-ph]]; Q. H. Cao, B. Yan and D. M. Zhang, Phys. Rev. D **92**, no. 9, 095025 (2015) [arXiv:1507.00268 [hep-ph]]; B. A. Dobrescu and Z. Liu, JHEP **1510**, 118 (2015) [arXiv:1507.01923 [hep-ph]]; J. H. Collins and W. H. Ng, arXiv:1510.08083 [hep-ph]; K. Das, T. Li, S. Nandi and S. K. Rai, Phys. Rev. D **93**, no. 1, 016006 (2016) [arXiv:1512.00190 [hep-ph]]; J. A. Aguilar-Saavedra and F. R. Joaquim, arXiv:1512.00396 [hep-ph]; M. Hirsch, M. E. Krauss, T. Opferkuch, W. Porod and F. Staub, arXiv:1512.00472 [hep-ph]; J. L. Evans, N. Nagata, K. A. Olive and J. Zheng, arXiv:1512.02184 [hep-ph]; J. Brehmer *et al.*, arXiv:1512.04357 [hep-ph]; A. Berlin, arXiv:1601.01381 [hep-ph].
- [12] G. Aad *et al.* [ATLAS Collaboration], JHEP **1512**, 055 (2015) [arXiv:1506.00962 [hep-ex]].
- [13] V. Khachatryan *et al.* [CMS Collaboration], Phys. Rev. D **91**, no. 5, 052009 (2015) [arXiv:1501.04198 [hep-ex]].
- [14] CMS Collaboration [CMS Collaboration], CMS-PAS-EXO-14-010.
- [15] G. Aad *et al.* [ATLAS Collaboration], JHEP **1507**, 162 (2015) [arXiv:1506.06020 [hep-ex]].
- [16] CMS Collaboration [CMS Collaboration], CMS-PAS-EXO-14-014.
- [17] V. Khachatryan *et al.* [CMS Collaboration], Phys. Lett. B **748**, 144 (2015) [arXiv:1501.05566 [hep-ex]].
- [18] R. N. Mohapatra, Phys. Rev. Lett. **56**, 561 (1986); R. N. Mohapatra and J. W. F. Valle, Phys. Rev. D **34**, 1642 (1986).
- [19] P. Minkowski, Phys. Lett. B **67**, 421 (1977); T. Yanagida, Conf. Proc. C **7902131**, 95 (1979); M. Gell-Mann, P. Ramond and R. Slansky, Conf. Proc. C **790927**, 315 (1979) [arXiv:1306.4669 [hep-th]]; S. L. Glashow, NATO Sci. Ser. B **59**, 687 (1980); R. N. Mohapatra and G. Senjanovic, Phys. Rev. Lett. **44**, 912 (1980).
- [20] A. Pilaftsis and T. E. J. Underwood, Nucl. Phys. B **692**, 303 (2004) [hep-ph/0309342]; J. Kersten and A. Y. Smirnov, Phys. Rev. D **76**, 073005 (2007) [arXiv:0705.3221 [hep-ph]]; Z. z. Xing, Prog. Theor. Phys. Suppl. **180**, 112 (2009) [arXiv:0905.3903 [hep-ph]]; X. G. He, S. Oh, J. Tandean and C. C. Wen, Phys. Rev. D **80**, 073012 (2009) [arXiv:0907.1607 [hep-ph]]; A. Ibarra, E. Molinaro and S. T. Petcov, JHEP **1009**, 108 (2010) [arXiv:1007.2378 [hep-ph]]; F. F. Deppisch and A. Pilaftsis, Phys. Rev. D **83**, 076007 (2011) [arXiv:1012.1834 [hep-ph]]; C. H. Lee,

- P. S. Bhupal Dev and R. N. Mohapatra, Phys. Rev. D **88**, no. 9, 093010 (2013) [arXiv:1309.0774 [hep-ph]].
- [21] P. S. B. Dev and R. N. Mohapatra, Phys. Rev. D **81**, 013001 (2010) [arXiv:0910.3924 [hep-ph]]; P. S. Bhupal Dev and R. N. Mohapatra, Phys. Rev. D **82**, 035014 (2010) [arXiv:1003.6102 [hep-ph]]; R. Lal Awasthi and M. K. Parida, Phys. Rev. D **86**, 093004 (2012) [arXiv:1112.1826 [hep-ph]].
- [22] H. Georgi, AIP Conf. Proc. **23**, 575 (1975); H. Fritzsch and P. Minkowski, Annals Phys. **93**, 193 (1975).
- [23] F. del Aguila and J. A. Aguilar-Saavedra, Nucl. Phys. B **813**, 22 (2009) [arXiv:0808.2468 [hep-ph]]; F. del Aguila and J. A. Aguilar-Saavedra, Phys. Lett. B **672**, 158 (2009) [arXiv:0809.2096 [hep-ph]]; F. del Aguila, J. A. Aguilar-Saavedra and J. de Blas, Acta Phys. Polon. B **40**, 2901 (2009) [arXiv:0910.2720 [hep-ph]].
- [24] C. Y. Chen and P. S. B. Dev, Phys. Rev. D **85**, 093018 (2012) [arXiv:1112.6419 [hep-ph]].
- [25] A. Das and N. Okada, Phys. Rev. D **88**, 113001 (2013) [arXiv:1207.3734 [hep-ph]].
- [26] A. Das, P. S. Bhupal Dev and N. Okada, Phys. Lett. B **735**, 364 (2014) [arXiv:1405.0177 [hep-ph]].
- [27] A. Das and N. Okada, arXiv:1510.04790 [hep-ph].
- [28] S. Chatrchyan *et al.* [CMS Collaboration], Phys. Rev. D **90**, 032006 (2014) [arXiv:1404.5801 [hep-ex]].
- [29] M. C. Gonzalez-Garcia and J. W. F. Valle, Phys. Lett. B **216**, 360 (1989).
- [30] S. C. Park, K. Wang and T. T. Yanagida, Phys. Lett. B **685**, 309 (2010) [arXiv:0909.2937 [hep-ph]]; C. S. Fong, R. N. Mohapatra and I. Sung, Phys. Lett. B **704**, 171 (2011) [arXiv:1107.4086 [hep-ph]].
- [31] E. Ma, Phys. Rev. D **80**, 013013 (2009) [arXiv:0904.4450 [hep-ph]]; F. Bazzocchi, D. G. Cerdeno, C. Munoz and J. W. F. Valle, Phys. Rev. D **81**, 051701 (2010) [arXiv:0907.1262 [hep-ph]]; S. C. Park and K. Wang, Phys. Lett. B **701**, 107 (2011) [arXiv:1011.3621 [hep-ph]]; S. S. C. Law and K. L. McDonald, Phys. Lett. B **713**, 490 (2012) [arXiv:1204.2529 [hep-ph]].
- [32] The ATLAS collaboration, ATLAS-CONF-2015-070.
- [33] CMS Collaboration [CMS Collaboration], CMS-PAS-EXO-15-005.
- [34] Y. Zhang, H. An, X. Ji and R. N. Mohapatra, Nucl. Phys. B **802**, 247 (2008) [arXiv:0712.4218 [hep-ph]]; A. Maiezza, M. Nemevsek, F. Nesti and G. Senjanovic, Phys. Rev. D **82**, 055022 (2010) [arXiv:1005.5160 [hep-ph]]; S. Bertolini, A. Maiezza and F. Nesti, Phys. Rev. D **89**, no. 9, 095028 (2014) [arXiv:1403.7112 [hep-ph]].

- [35] A. Ferroglia, C. Greub, A. Sirlin and Z. Zhang, Phys. Rev. D **88**, 033012 (2013) [arXiv:1307.6900].
- [36] V. Khachatryan *et al.* [CMS Collaboration], JHEP **1408**, 173 (2014) [arXiv:1405.1994 [hep-ex]].
- [37] G. Aad *et al.* [ATLAS Collaboration], arXiv:1512.05099 [hep-ex].
- [38] G. Aad *et al.* [ATLAS Collaboration], Phys. Lett. B **737**, 223 (2014) [arXiv:1406.4456 [hep-ex]].
- [39] G. Aad *et al.* [ATLAS Collaboration], Eur. Phys. J. C **75**, 69 (2015) [arXiv:1409.6190 [hep-ex]].
- [40] G. Aad *et al.* [ATLAS Collaboration], Eur. Phys. J. C **75**, no. 5, 209 (2015) [Eur. Phys. J. C **75**, 370 (2015)] [arXiv:1503.04677 [hep-ex]].
- [41] V. Khachatryan *et al.* [CMS Collaboration], JHEP **1408**, 174 (2014) [arXiv:1405.3447 [hep-ex]].
- [42] F. Dias, S. Gadatsch, M. Gouzevich, C. Leonidopoulos, S. Novaes, A. Oliveira, M. Pierini and T. Tomei, arXiv:1512.03371 [hep-ph].
- [43] The ATLAS collaboration, ATLAS-CONF-2015-068; ATLAS-CONF-2015-071; ATLAS-CONF-2015-073; ATLAS-CONF-2015-075.
- [44] CMS Collaboration [CMS Collaboration], CMS-PAS-EXO-15-002.
- [45] J. Alwall *et al.*, JHEP **1407**, 079 (2014) [arXiv:1405.0301 [hep-ph]].
- [46] Q. H. Cao, Z. Li, J. H. Yu and C. P. Yuan, Phys. Rev. D **86**, 095010 (2012) [arXiv:1205.3769 [hep-ph]].
- [47] T. Jezo, M. Klasen, D. R. Lamprea, F. Lyonnet and I. Schienbein, JHEP **1412**, 092 (2014) [arXiv:1410.4692 [hep-ph]].
- [48] G. Aad *et al.* [ATLAS Collaboration], arXiv:1512.01530 [hep-ex].
- [49] V. Khachatryan *et al.* [CMS Collaboration], arXiv:1512.01224 [hep-ex].
- [50] V. Khachatryan *et al.* [CMS Collaboration], arXiv:1509.06051 [hep-ex].
- [51] M. E. Peskin and T. Takeuchi, Phys. Rev. Lett. **65**, 964 (1990).
- [52] K. Hsieh, K. Schmitz, J. H. Yu and C.-P. Yuan, Phys. Rev. D **82**, 035011 (2010) [arXiv:1003.3482 [hep-ph]].
- [53] J. Pumplin, D. R. Stump, J. Huston, H. L. Lai, P. M. Nadolsky and W. K. Tung, JHEP **0207**, 012 (2002) [hep-ph/0201195].

- [54] T. Sjostrand, S. Mrenna and P. Z. Skands, JHEP **0605**, 026 (2006) [hep-ph/0603175].
- [55] S. Ovin, X. Rouby and V. Lemaitre, arXiv:0903.2225 [hep-ph]; J. de Favereau *et al.* [DELPHES 3 Collaboration], JHEP **1402**, 057 (2014) [arXiv:1307.6346 [hep-ex]].
- [56] M. Cacciari, G. P. Salam and G. Soyez, JHEP **0804**, 063 (2008) [arXiv:0802.1189 [hep-ph]]; M. Cacciari, G. P. Salam and G. Soyez, Eur. Phys. J. C **72**, 1896 (2012) [arXiv:1111.6097 [hep-ph]].